CivilEng

MDPI

Article

Behavior of Reinforcing Bar Connection of Hollow-Core Slabs to Steel Beams under In-Plane Forces

Susana Hernandez Brito [1], Karam Mahmoud [2] and Ehab F. El-Salakawy [3,*]

[1] Structural Engineer-In-Training, Hatch Canada Inc., Winnipeg, MB R3C 3Z5, Canada
[2] Structural Engineer, Charleson Engineering Ltd., Winnipeg, MB R3T 2A7, Canada
[3] Department of Civil Engineering, University of Manitoba, Winnipeg, MB R3T 5V6, Canada
* Correspondence: ehab.el-salakawy@umanitoba.ca

Abstract: Hollow-core slab (HCS) floors supported on steel beams require the use of steel reinforcement as connections to avoid slab displacement caused by lateral loads. However, current North American design codes offer limited provisions on the design and behavior of such connections. In this study, the results of an experimental investigation conducted on such connections to assess their capacity and mode of failure are presented. Eleven full-scale assemblies of HCS reinforcing bar connections to steel beams were tested to failure under monotonic in-plane loading (compression, tension, or shear). Test results revealed that connections tested under compression failed by bar buckling without yielding. Under tension, the connection bar reached close-to-yielding or yielding strains at the unrestrained portion of the bar, followed by grout splitting in the shear key or the grouted core. Finally, the mechanism of failure of specimens subjected to shear was governed by bar yielding.

Keywords: hollow-core slabs; in-plane forces; integrity ties; end-bearing connection; side-bearing connections

check for updates

Citation: Brito, S.H.; Mahmoud, K.; El-Salakawy, E.F. Behavior of Reinforcing Bar Connection of Hollow-Core Slabs to Steel Beams under In-Plane Forces. *CivilEng* **2022**, *3*, 831–849. https://doi.org/10.3390/civileng3040048

Academic Editor: Hugo Rodrigues

Received: 20 June 2022
Accepted: 21 September 2022
Published: 25 September 2022

1. Introduction

Approximately 1.83 million m^2 of hollow-core slabs (HCSs) are produced each year in Canada [1]. Designers often choose such HCSs to cover long spans owing to their structural efficiency. The voids inside these slabs eliminate up to 50% of the concrete volume associated with using solid slabs of equal thickness, which results in relatively lighter elements. The use of prestressed concrete further reduces deflections and minimizes section height. Depending on the thickness, HCSs can span up to 17 m without intermediate supports. Moreover, the HCSs are convenient for construction purposes to allow for more floor clearance. The interior cores are commonly employed for thermal and noise isolation or run mechanical, electrical, and plumbing conduits. Therefore, these slabs are optimal for clear and open spaces in residential and office buildings.

Floors constructed with HCSs are typically designed as continuous horizontal diaphragms, which transfer in-plane lateral loads to the supporting structure throughout their bearing connections [2]. The in-plane lateral loads (e.g., wind/seismic loads, accidental loads during construction, vibrations, or movements of the supports) cause in-plane axial or shear forces at the bearing connections of the HCS floors to supporting members (Figure 1). Based on the load transfer (web) direction of HCSs, two types of connection-to-steel beam supports are identified according to the CPCI design manual [3]: end-bearing and side-bearing connections. In both types of connections, steel reinforcement is either welded or tied to the steel supporting beam on one side. On the other side, this reinforcement is either inserted at the grouted joint between HCS, for end-bearing connections, or in saw-cut pockets on the side of the slab, for side-bearing connections. The steel reinforcement in such connections is also necessary to tie the slabs to their supporting structure, prevent slabs displacements and preserve the structural integrity of buildings utilizing such

HCS floors [3–6]. Inadequate connection reinforcement may result in floor misalignments or loss of bearing of the HCS units.

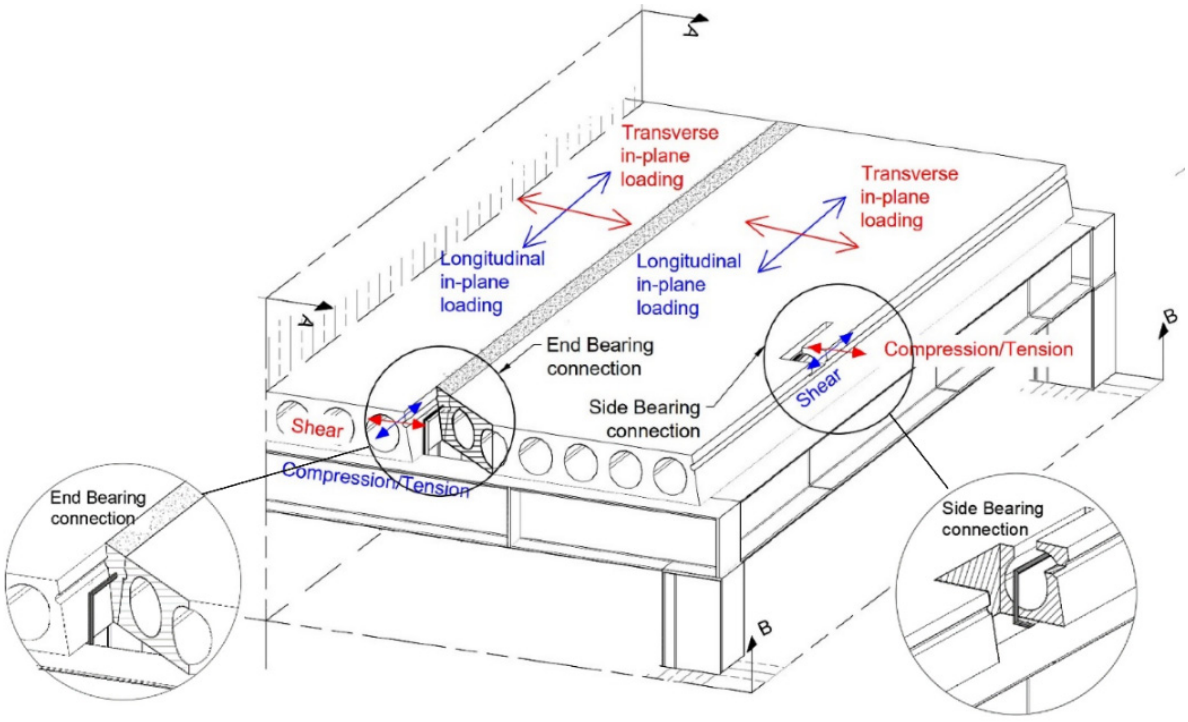

Figure 1. Forces on end- and side-bearing connections of HCS supported on steel beams.

Current design codes, ACI 318-19 [4] and CSA A23.3-19 [5], refer to the bearing connection reinforcement as "integrity ties" owing to their main function in HCS floors. According to CSA A23.3-19 [5] and ACI 318-19 [4], integrity ties in end-bearing connections shall ensure a minimum specified tensile strength of 5.0 and 4.4 kN/m of the bearing length of HCS on the supporting beam, respectively, or 2.5% of the service loads [2]. These specifications are intended to ensure the minimum level of structural integrity of the HCS floor diaphragm. However, these requirements do not supersede acting lateral forces in HCS floor diaphragms. If the resultant tension forces from the in-plane forces acting on the diaphragm are greater than the code-specified values, proper steel detailing and tie spacing must be provided to carry these forces. It is to be noted that the required minimum capacity in the codes is set solely for tension forces acting on integrity ties in end-bearing connections. Given the reversible nature of the in-plane loads acting on HCS floor diaphragms (e.g., wind or seismic), compression and transverse (i.e., shear) forces are as likely to be acting on end and side-bearing connections as tension forces. Therefore, connections must resist these forces to ensure the structural integrity of buildings and reach bar yielding before peak load; providing ample warning before failure. In addition, integrity ties in HCS floor diaphragms may be used to brace the top flange of the supporting steel beam, which carries the flexural compressive stresses under gravity loads [2]. In these situations, the designer must provide a tie spacing that allows each individual tie to develop the nominal tensile yield capacity while ensuring a minimum level of floor integrity [2], which shall not exceed 3000 mm [3,4].

There is a noticeable gap in the North American codes on design provisions of reinforcing bars as connections for the structural integrity of HCS floors. For instance, the CPCI design manual [3] and the CSA A23.3-19 standards [5] recommend using the shear friction theory to calculate the reinforcement ratio (A_{vf}) necessary for HCS bearing connections or estimate the capacity (V_f) of a given connection detailing under in-plane forces. However, this approach might not be appropriate for this specific type of integrity ties, which has an eccentricity regarding the points of load application and the resultant force (Figure 2) and

contains free portions of the bar not embedded in concrete or grout. Therefore, designers neglect any contribution from friction interlock when computing the resistance of each individual tie, which the tie spacing depends on. Providing an accurate value of load capacity would increase the refinement in design calculations of tie spacing.

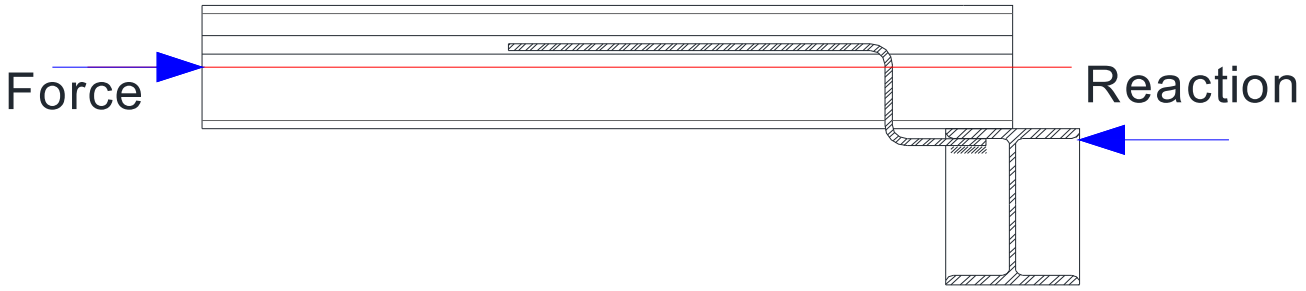

Figure 2. Eccentricity of the load application in relation to the reaction.

Lam et al. [7] and Lam [8] investigated a system where the composite action of HCS with steel beams was carried out by headed studs and straight ties, as reinforcement, and concrete topping and void infill cast integrally. The headed studs are welded to the upper side of the top flange of the beam, while the ties are inserted into saw-cut milled slots in the flanges of the HCS and extended to the contiguous slab. Finally, these milled slots are filled with concrete [7].

Based on previous investigations [7], Lam [8,9] proposed a design equation for the shear capacity of headed studs under in-plane forces, which depends primarily on the modulus of elasticity and compressive strength of the concrete infill, the tensile strength and height/diameter ratio of the headed-stud, the diameter of the transverse reinforcement and the gap between contiguous HCS. Although the detailing of this connection serves to preserve floor integrity against lateral forces, the main function of the system is to ensure the composite action between the HCS floor and the supporting beam. Hence, the load capacity of this connection cannot be compared to that of the reinforcing bar connection.

In Eastern Canada, the connection reinforcement or integrity tie consists of a 10 M "Z-shaped" (400 W) steel bar, as shown in Figure 3. In practice, this connection bar has a minimum embedment length in grout of 450 mm to ensure adequate anchorage, while the other end, approximately 120-mm long, is welded to the underside of the top flange of the steel beam with a minimum welding length of 50 mm. This leaves a 70 mm long portion of the bar unrestrained (Figure 4). This connection detailing is more commonly used because of their low cost, convenience, and fast installation. However, to date, there are no reported studies on the capacity or the mode of failure of the reinforcing bar connection. Hence, it is uncertain whether the reinforcing bar connection meets the intent of the code of developing the full tensile yielding strength of the ties or satisfy code requirement for structural integrity. Therefore, this study investigates the mode of failure and the in-plane load capacity of the integrity ties in HCS connections to steel beams, which are commonly used in Eastern Canada [10].

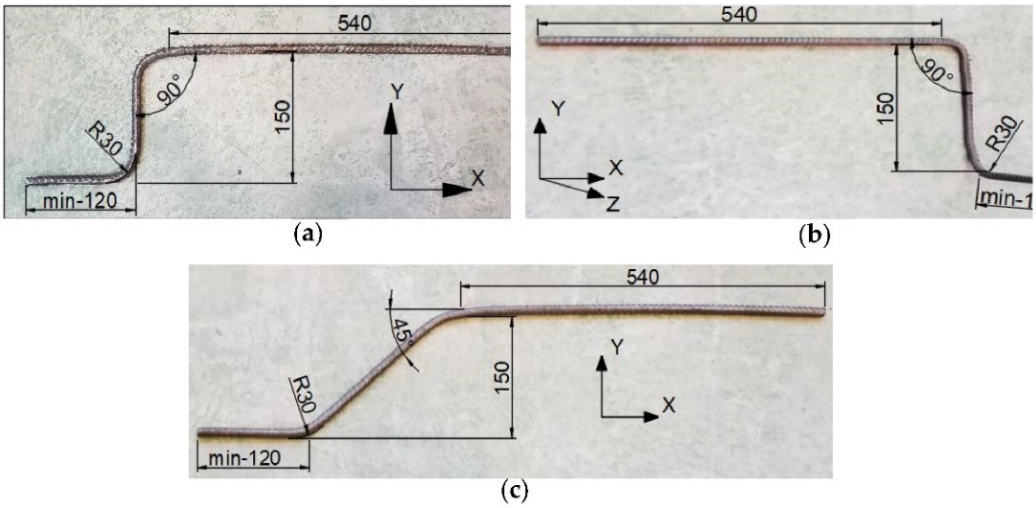

Figure 3. Connection bar details (size 10 M): (**a**) 90-degree bends for end bearing connection, (**b**) 90-degree bends for side bearing connection, and (**c**) 45-degree bends for end bearing connection (Dimensions in mm).

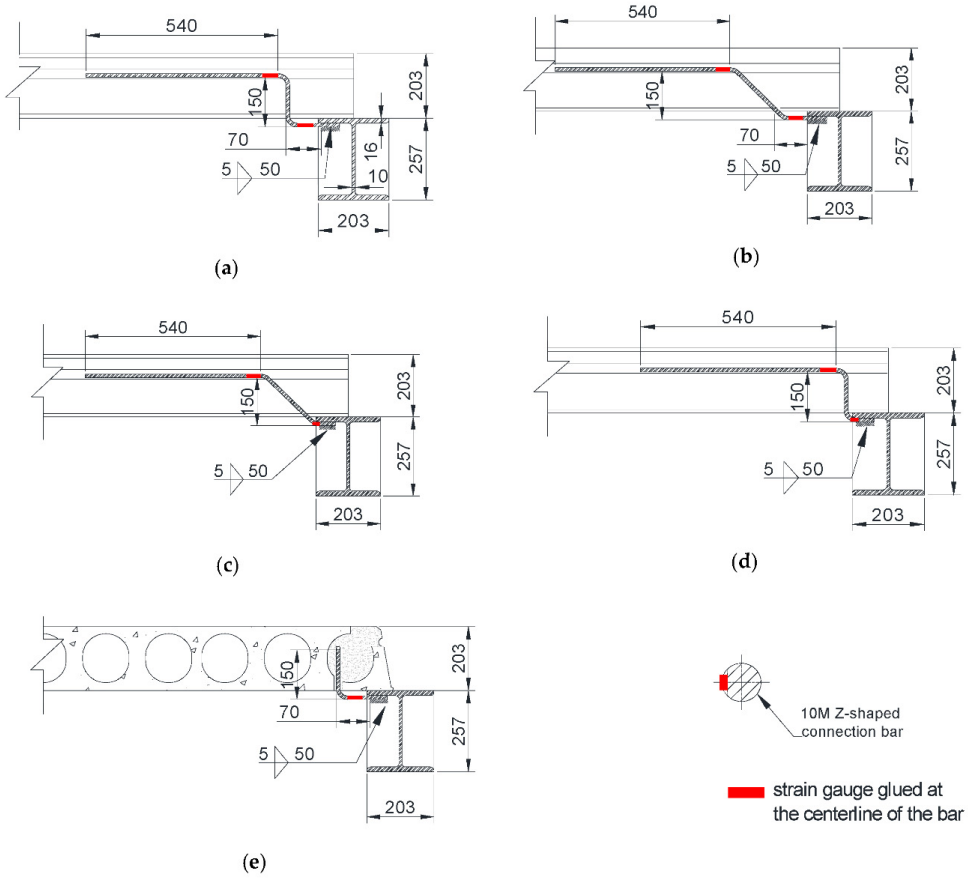

Figure 4. Steel bar connection detailing and locations of strain gauges (all dimensions in mm): (**a**) 90-degree bend bar—end-bearing connection; (**b**) 45-degree bend bar—end-bearing connection; (**c**) Reduced unrestrained bar length for 45-degree bend bar (EB-CN-45R); (**d**) Reduced unrestrained bar length for 90-degree bend bar (EB-CN-90R); and (**e**) 90-degree bend bar—side-bearing connections. (Dimensions in mm).

2. Research Significance

Hollow-core slab floors are usually designed as diaphragms to resist in-plane loads in large-span buildings [3]. They are often connected with 10 M Z-shaped reinforcing bars (integrity ties) to their supporting steel beams [10]. However, the capacity of the connection bar and the mode of failure are not investigated. In this study, the behavior and capacity of both end-bearing and side-bearing Z-shaped 10 M bar connections are evaluated under different loading conditions (tension, compression, or shear forces). The results of this pioneer investigation serve to enhance the confidence of using such connections and explore refined connection detailing to reach higher capacities.

3. Experimental Program

3.1. Test Specimens

Eleven full-scale specimens were assembled and tested under monotonic in-plane forces until failure. The specimens were divided into two series based on the type of bearing. Series I, which contained seven specimens, was dedicated to investigating end-bearing connections, while Series II comprised four side-bearing specimens. The specimens were constructed using 203 mm thick HCS that were cut to 1220 mm square segments. Each end-bearing specimen consisted of two HCS segments, while side-bearing connections were constructed using one HCS segment. These HCS segments were supported on and connected to a W250 $\times$ 67 steel beam using a "Z-shaped", 10 M steel reinforcing bar as indicated in Figures 3 and 4. On one side, this reinforcing bar was welded to the underside of the top flange of the beam while the other side was grouted to the joint (shear key) between HCS segments.

The test variables included the direction (pulling or pushing against the supporting beam) and orientation (normal or parallel to the axis of the supporting beam) of the applied in-plane force. These test variables account for all possible in-plane horizontal forces and bearing types in HCS floors supported on steel beams. In addition, the effect of bar bends and reduced unrestrained length of the connection bar for end-bearing specimens was investigated.

The reinforcing bar, currently used in construction practice, is commonly shaped with 90-degree bend angles, as shown in Figure 3a,b [10]. However, an alternative 45-degree bend angle connection bar was included in this study for end-bearing connections (Figure 3c), to evaluate the effect of reducing bar bends. Bars with a 45-degree bend are expected to resist a higher load than the 90-degree bends bars since the 45-degree bent portion provides a horizontal resistance component at the bent points, which is negligible in their counterparts with 90-degree bend. Finally, reduced unrestrained length connection bars for the 90-degree and 45-degree bend angles were introduced to evaluate the effect of reducing the unrestrained length on the capacity of the connection. The details of these connections are shown in Figure 4.

The specimen nomenclature consists of three parts. The first part refers to the type of bearing where "EB" and "SB" stand for end-bearing and side-bearing, respectively. The second part consists of two letters denoting the load direction ("C" for compression/pushing or "T" for tension/pulling) and load orientation ("N" or "P" for normal or parallel to the longitudinal axis of the supporting beam, respectively). The last part of specimen nomenclature refers to the bend angles of the reinforcing bar ("45" or "90"-degrees). In addition, for the specimens with reduced unrestrained length, the letter "R" was added at the end of the nomenclature. Table 1 lists the test specimens.

A seating (bearing) length of 75 mm was provided in all HCS, which exceeds the minimum requirements of 50 mm as per the Canadian standards CSA A23.3-19 [5] and CPCI design manual [3]. This seating length was provided to ensure the failure of the connection while the HCS remains bearing on the steel beam. Additionally, in case of end-bearing, the spacing (joint) between the two HCS segments was set to fit the connection bar tightly, as performed in the construction practice.

Table 1. Test Specimens.

Series	Type of Bearing	Specimen ID	Load Direction/ Orientation	Bend Angles (Degrees)
Series I	End-Bearing	EB-CN-90	Pushing/Normal	90
		EB-CN-90R		90 R *
		EB-CN-45		45
		EB-CN-45R		45 R *
		EB-TN-90	Pulling/Normal	90
		EB-TN-45		45
		EB-CP-90	Pushing/Parallel	90
Series II	Side-Bearing	SB-CN-90	Pushing/Normal	90
		SB-TN-90	Pulling/Normal	90
		SB-CP-90	Pushing/Parallel	90
		SB-TP-90	Pulling/Parallel	90

* R stands for reduced unrestrained length of reinforcing bar with either 90- or 45-degree bends

3.2. Material Properties

The tensile properties of the steel bars were obtained by standard tests according to the ASTM A370 [11]. The 10 M steel bar has a strength and strain at yielding of 470 ± 8 MPa and 2370 ± 40 με, respectively, with a modulus of elasticity of 199 GPa. A commercially available grout was used to fill in the joints between the HSC units or the cores of the slabs in which the 10 M bar was embedded. This normal-strength grout (20–25 MPa) was mixed, poured, and cured as per the manufacturer's guidelines. The compressive strength of the grout mix tested according to the ASTM C109/C109M-20 [12] on the day of testing was 25.1 ± 3.1 MPa. The HCS were cast at the supplier facility using a concrete mix with a target 28-day compressive strength of 55–60 MPa. These slabs were reinforced with 7–12.7 mm Grade 1860 MPa prestressing strands, which presents a reinforcement ratio of 0.493%.

3.3. Test Setup and Instrumentation

The test setup consists of three main elements: (1) clamping beams to attach the slabs to the actuator and distribute the in-plane forces uniformly along the edge of the slab; (2) vertical link supports (pinned-pinned), which carry half the self-weight of the slabs and allow for the lateral displacement of the slab; and (3) the supporting steel beam, where the connection bar is welded. Figure 5 shows the details of the test setup. For specimens tested under parallel loading (shear), two rollers were welded to the beam to guide the slabs and prevent rotation, as shown in Figure 5d.

The load was applied to the slab to generate an in-plane force that is normal or parallel to the supporting beam. The normal force was either pushing or pulling such that the connection bar is under compression or tension forces, respectively. The parallel force was always pushing or pulling to generate a shear force in the connection bar. A similar testing method was previously used by Mejia-McMaster and Park [13]. No gravity loads, other than the self-weight of the slab, were added to the loading scheme representing the lower bound case of minimum friction between the HCS and the supporting beam. The monotonic load was applied using a hydraulic actuator with a 500 kN load and 130 mm stroke capacities. This actuator was mounted on a strong triangular reaction frame. A displacement-controlled loading rate of 5.0 mm/min was used to allow for load accommodation and test duration of about 25–30 min [14], assuming a connection capacity of 40 kN.

Slab displacement was measured using linear variable displacement transducers (LVDTs), as shown in Figure 5. The strains in the connection bar at its bends was measured by electrical strain gauges (Figure 4). The applied load was recorded with a load cell installed at the tip of the actuator. The readings of this instrumentation were processed

through a Data Acquisition (DAQ) System and stored on a personal computer. In addition, cracking propagation or spalling, if any, were carefully marked and recorded during testing.

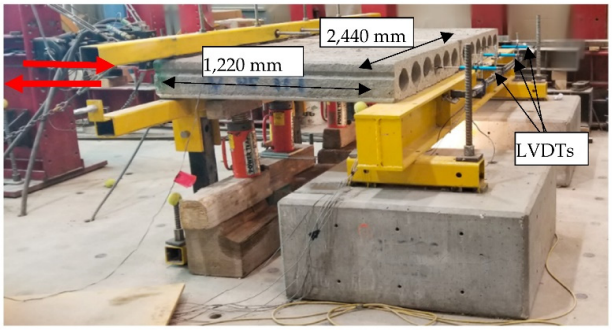

(**a**)

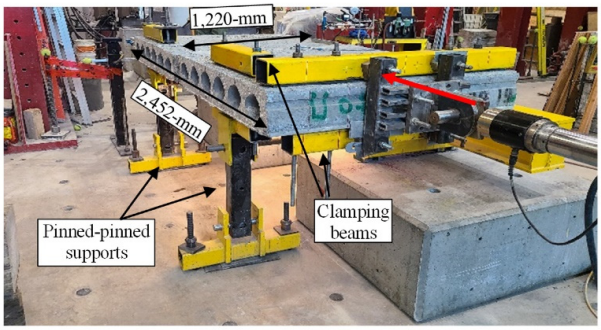

(**b**)

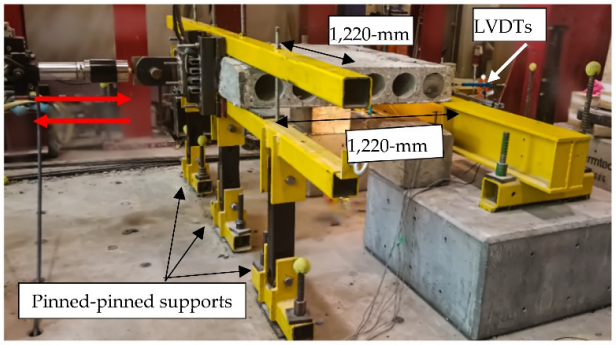

(**c**)

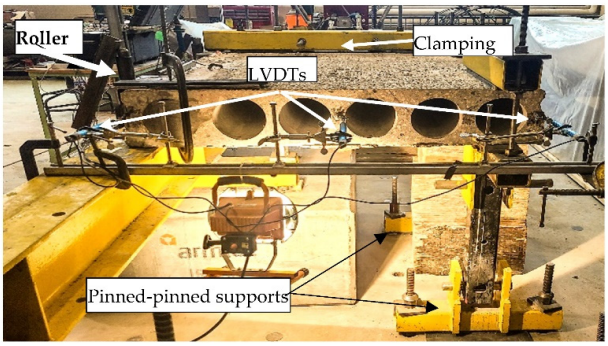

(**d**)

Figure 5. Test setup and external instrumentation: (**a**) normal load on end end-bearing specimen, (**b**) parallel load on end end-bearing specimen, (**c**) normal load on side-bearing specimen, and (**d**) parallel load on side-bearing specimen (Dimensions in mm).

4. Test Results and Discussion

This section introduces and discusses the experimental results in terms of mode of failure, capacity, measured strains, deflections, and overall structural integrity. In addition, the effects of decreasing the bend angle of the connection bar to 45-degree and/or reducing the unrestrained length of the bar are discussed. Table 2 lists a summary of the test results.

Table 2. Summary of test results.

Series	Type of Bearing	Specimen ID	Load Direction/ Orientation	Mode of Failure	Yielding Load (kN)	Peak Load (kN)	Strains at Peak Load (με)	Slab Displacement at Peak Load (mm)
Series I	End-Bearing	EB-CN-90	Pushing/Normal	Bar buckling	-	12.6	−1050	3.9
		EB-CN-90R		Bar buckling	-	13.7	−1460	4
		EB-CN-45		Bar bending	-	16.3	−1010	3.9
		EB-CN-45R		Bar buckling	17.1	17.1	−2770	3.9
		EB-TN-90	Pulling/Normal	Bar yielding & grout splitting	30.3	30.3	2370	22.6
		EB-TN-45			37.2	53.2	24,980	21.8
		EB-CP-90	Pushing/Parallel	Bar yielding	9.2	15.3	8080	60.3
Series II	Side-Bearing	SB-CN-90	Pushing/Normal	Bar buckling	-	11.4	900	3.5
		SB-TN-90	Pulling/Normal	Bar yielding & grout splitting	36.3	46	13,410	22.9
		SB-CP-90	Pushing/Parallel	Bar yielding	9.7	16.1	9330	60.5
		SB-TP-90	Pulling/Parallel	Bar yielding	31.7	34.8	3350	63.8

4.1. Mode of Failure

4.1.1. Specimens of Series I—End-Bearing Connections

Loading Normal to the Axis of the Supporting Beam

The load direction, pulling or pushing, applied normal to the supporting beam resulted in different modes of failure in the connection bar. Under tension forces (pulling), the Z-shaped bar failed by steel yielding at the unrestrained portion of the bar near the bend, followed by grout splitting. In addition, the bottom bend of the connection bar straightened and elongated, regardless of the bend angle (Figure 6a,b). The end-bearing specimen with a 45-degree bent bar (EB-TN-45) exhibited bar yielding and later, bar necking (Figure 6b). Afterwards, a single crack appeared at the grouted joint above the connection bar for both specimens tested under a normal pulling force. In contrast, the end-bearing specimen with a 90-degree bent bar (EB-TN-90) experienced an early cracking due to bond failure between the HCS and the grouted shear key (Figure 6a).

A hairline crack was observed at approximately 83% of the maximum load in the grouted shear-key in specimen EB-TN-90. Near peak load, the connection bar reached close-to-yielding strains. The crack in the shear key of both specimens (EB-TN-90 and EB-TN-45) started with grout spalling around the bar and propagated longitudinally across the shear key. This crack extended across the grouted joint until splitting occurred, as depicted in Figure 6.

Under compression forces (pushing/CN), the mode of failure of end-bearing specimens was governed by bar bending or buckling at the bottom bend (Figure 7a–d). In general, the connection bar did not yield before the maximum load, except for specimen EB-CN-45R, in which the connection bar developed yielding strains at the bottom bend before bar buckling. The bars were gradually bent or buckled in the direction of the force. While the bars with 90-degree bends in end-bearing specimens (EB-CN-90 and EB-CN-90R) buckled to the front, forming a 180-degree bend shape (Figure 7a,c), the unrestrained portion of the bar in specimen EB-CN-45 bent downwards, as shown in Figure 7b. Then, the slabs gradually pulled the unrestrained (free) portion of the connection bar, provoking "dragging" in the bar. The load started to drop gradually, while the bar experienced further bending or buckling. At 50% of the peak load, bar rupture occurred near the welding in specimens EB-CN-90 and EB-CN-90R. For specimen EB-CN-45, no bar rupture was observed after the slabs were displaced excessively (56.8 mm). No cracking was observed in the slabs or the grouted shear key at any point during the test of these specimens.

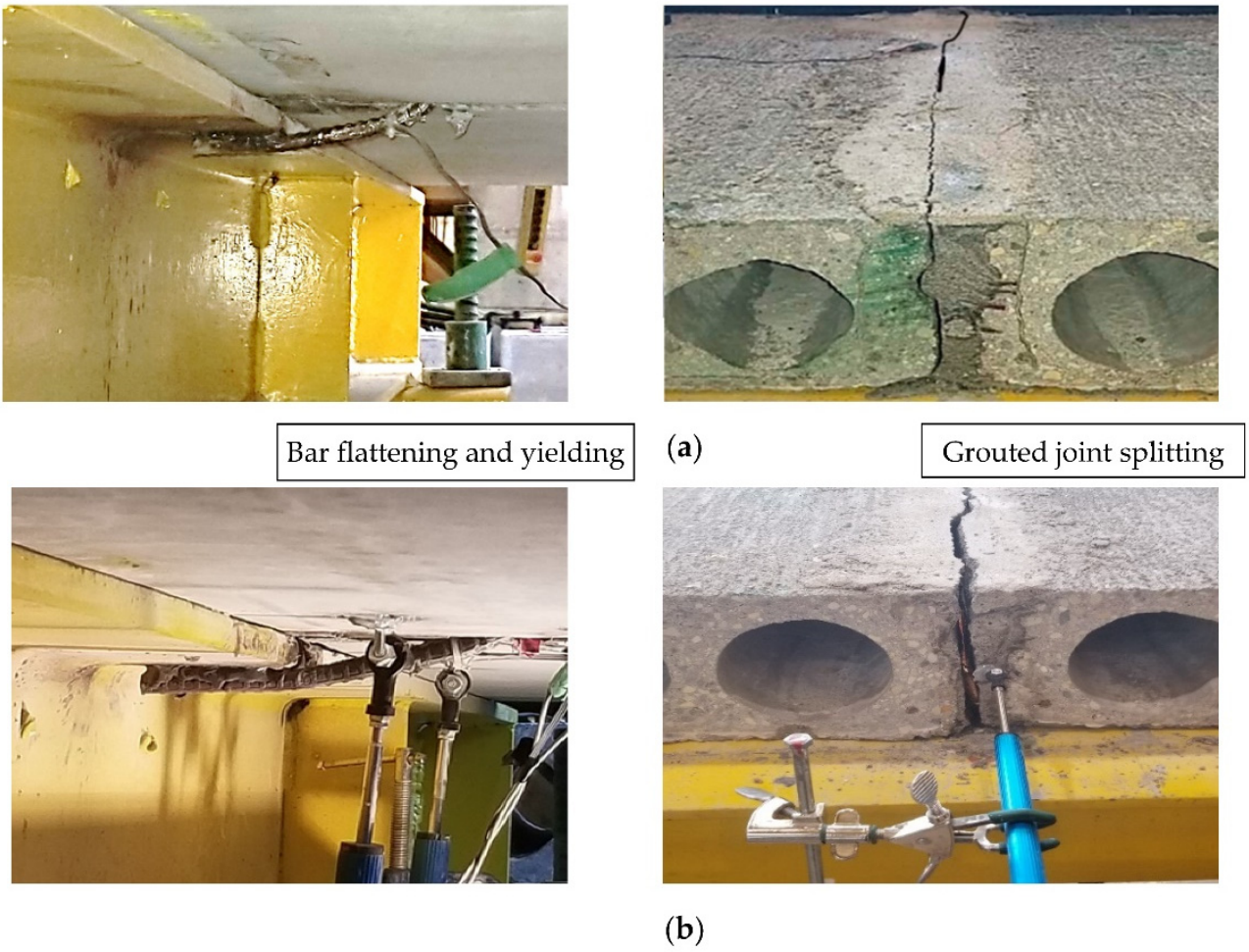

Figure 6. Mode of failure for end-bearing specimens tested under axial pulling (tension forces): (**a**) EB-TN-90 (pulling/normal), and (**b**) EB-TN-45 (pulling/normal).

Although the connection with a 45-degree bent bar and reduced unrestrained length (EB-CN-45R) buckled and experienced load drop, it was the only one tested under compression that reached yielding strain before the peak load. This indicated that the combined effects of reducing the unrestrained length and decreasing the angle of bar bends improved the behavior, where a more desirable mode of failure in the connection bar was observed.

Loading Parallel to the Axis of the Supporting Beam

The end-bearing specimen tested under a pushing force (EB-CP-90) failed due to bar yielding followed by bar rupture near the weld (Figure 7e). At the early stages of loading, the connection demonstrated bar kinking and elongation in the direction of the force, followed by yielding and further deformation of the bar. Before the peak load, the connection bar experienced twisting, which resulted in bar shear off near the weld after undergoing excessive deformation.

4.1.2. Specimens of Series II—Side-Bearing Connection

Loading Normal to the Axis of the Supporting Beam

Under tension forces (pulling), the side-bearing specimen with the currently used connection detailing (SB-TN-90) experienced a similar mode of failure to EB-TN-45. After bar yielding and straightening, the grout started to crack, and the specimen failed by grout splitting (Figure 8a). However, the connection bar did not reach the necking stage and the cracking pattern was different from other test specimens. The crack started around the connection bar, but it propagated transversely to the direction of load application

across the grouted core towards the top surface of the slab. Finally, the two HCS segments split at the grouted joint.

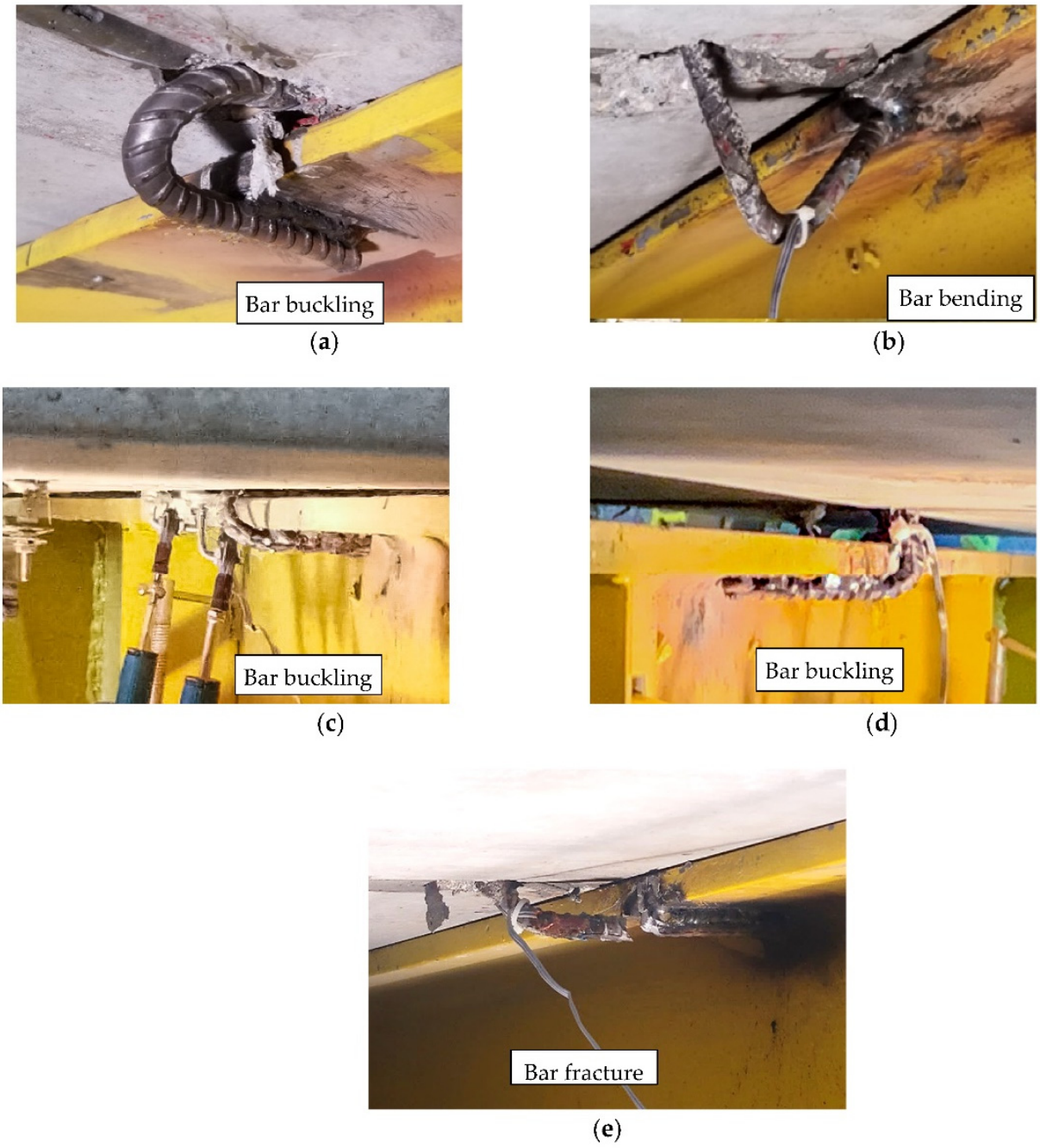

Figure 7. Mode of failure for end-bearing specimens tested under pushing forces (parallel and normal): (**a**) EB-CN-90 (pushing/normal), (**b**) EB-CN-45 (pushing/normal), (**c**) EB-CN-90R (pushing/normal), (**d**) EB-CN-90R (pushing/normal), and (**e**) EB-CP-90 (pushing/parallel).

When tested under compression (pushing), the side-bearing connection (SB-CN-90) demonstrated a similar failure mechanism to that of its end-bearing counterpart specimen (EB-CN-90), however, no bar rupture occurred. The test was halted after a load drop of 70% of the maximum load and noticeable bar distortion (Figure 8b).

Loading Parallel to the Axis of the Supporting Beam

The side-bearing connection (SB-CP-90), tested under pushing force, showed similar behavior to its end-bearing counterpart. The connection bar failed owing to bar kinking and yielding with excessive deformation. However, in this specimen, no bar twisting, or bar rupture was observed (Figure 8c). Conversely, when tested under pulling, the connection bar in specimen SB-TP-90 failed because of bar yielding followed by bar twisting and necking near the welding point (Figure 8d). In both cases, the testing was also halted after significant bar deformation and no further strength gain.

4.2. Connection Load Capacity

The expected load capacity of 10 M steel bars with a nominal yield strength of 400 MPa is 40 kN given that the bar cross-sectional area is 100 mm^2 and no material resistance factor is applied. Typically, a 10 M connection bar is installed in every grouted shear key of the slabs, resulting in a tie spacing of 1.22 m for HCS and thereof, an expected capacity of 32.8 kN/m in tension (corresponding to the yielding load of the bar). North American design codes [4,5] specify a minimum capacity in tension for integrity ties of 5.0 and 4.4 kN/m of supported slab length, respectively. If the connection bar can develop the expected nominal tensile yielding strength, as the code intent, the connection capacity would be 6.6 times larger than the specified values given a spacing of 1220 mm. Figure 9 depicts the capacity for all test specimens, as well as the yielding load, if applicable. The threshold of expected capacity based on the connection bar properties and the above-mentioned code limits are also indicated in Figure 9.

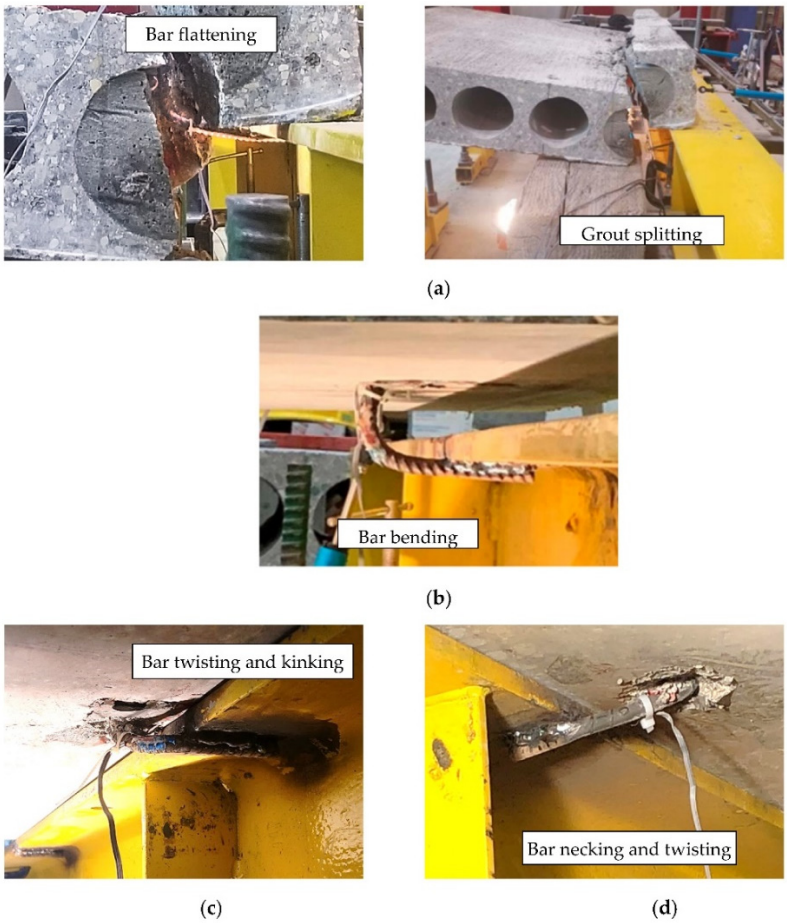

Figure 8. Mode of failure for side-bearing specimens: (**a**) SB-TN-90 (pulling/normal), (**b**) SB-CN-90 (pushing/normal), (**c**) SB-CP-90 (pushing/parallel), and (**d**) SB-TP-90 (pulling/parallel).

4.2.1. Specimens of Series I—End-Bearing Connection
Loading Normal to the Axis of the Supporting Beam

The load direction affected the mode of failure and load capacity of connections. End-bearing connections tested under tension (pulling) had a desirable mode of failure, where the connection bars yielded followed by cracking in the grouted shear-key. End bearing specimens EB-TN-45 and EB-TN-90 had a peak load of 53.2 kN and 30.3 kN, at 21.8 and 22.6 mm of displacement, respectively. The relatively lower load capacity in the latter specimen can be attributed to the early splitting failure of the grout. Both connection details met the code specifications [4,5] for integrity ties with supporting members other than bearing walls and the yielding load was close to expected values.

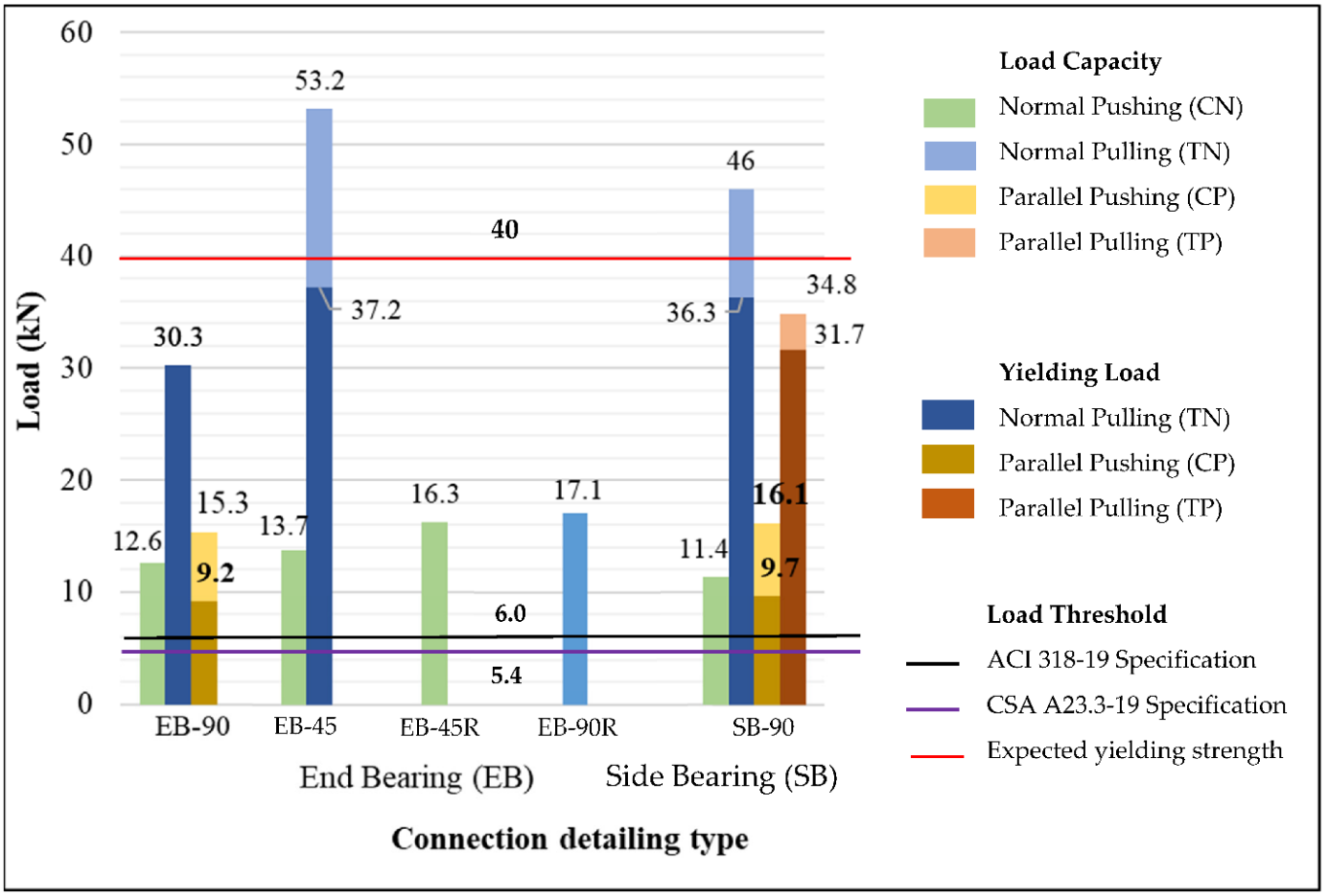

Figure 9. Connection capacity.

In contrast, end-bearing connections tested under compression exhibited less than half the capacity of their counterparts under tension forces due to bar bending or buckling, without developing the yielding strength of the bar. Specimens EB-CN-90 and EB-CN-45 attained a capacity of 12.6 kN and 16.3 kN, respectively, at a displacement of 3.9-mm, which indicates that the bar was at the early stages of its linear-elastic behavior when bending started. These results also demonstrated that decreasing the bend angle from 90 to 45-degree resulted in a 29% increase in the load capacity. However, minimizing the unrestrained length of the bar, in end-bearing connections with either 90 or 45-degree bar bends, did not significantly increase the connection capacity. Specimens EB-CN-90R and EB-CN-45R reached a capacity of 13.7 and 17.1 kN, respectively. This represents an 8.0 and 5.0% increase in the load capacity compared to their counterparts with the unrestrained length of 70 mm, respectively.

Loading Parallel to the Axis of the Supporting Beam

The capacity attained in the end-bearing specimen (EB-CP-90), tested under parallel pushing load, achieved similar capacity compared to its counterpart tested under axial forces. However, the peak capacity was 15.3 kN after the slabs displaced 60.3 mm, resulting from kinking of the unrestrained bar portion. This indicated that the bar had a relatively poor response to the pushing force when the load is applied parallel to the support (shear).

4.2.2. Specimens of Series II—Side-Bearing Connection

Loading Normal to the Axis of the Supporting Beam

Similar to specimens of Series I, the capacity of side-bearing specimens under normal loading depends on the loading direction. A larger load capacity was observed in specimens under tension compared to those tested under compression. While the side-bearing specimen tested under tension forces (SB-TN-90) reached a capacity of 46.0 kN, the peak load for the specimen tested under compression was 11.4 kN.

Loading Parallel to the Axis of the Supporting Beam

Side-bearing specimens tested under parallel loading also exhibited larger load capacity when being pulled than when being pushed. Specimen SB-TP-90 tested under pulling attained a maximum load capacity of 34.8 kN. In contrast, the side-bearing connection SB-CP-90, tested under pushing, reached a load capacity of 16.1 kN, which is less than half the capacity of its counterpart tested under a pulling force.

The connection capacities, depicted in Figure 9, demonstrated that for all bearing connections (Series I and II), the bar was more vulnerable under pushing forces, regardless of the load orientation (parallel or normal to the supporting beam) than under pulling forces. Under pushing axial forces, the eccentricity of the applied load with respect to the reaction point at the bottom of the beam flange (Figure 2), triggered an early bending/buckling of the connection bar at the bend. In the case of the specimens tested under parallel forces, the force was transferred to the supporting beam with an additional horizontal eccentricity (unrestrained portion), which resulted in the peak load being reached at very large displacements (60.3 mm). These load eccentricities caused a significant reduction in the capacity.

4.3. Strains in the Connection Bar

Figure 9 presents the load-strain relationship for the connection bar at the unrestrained bend in specimens from Series I and II, respectively. It is to be noted that the strain gauge attached to the grouted side of the connection bar did not read strains larger than 400 με in any specimen. As such, its readings are not presented in this paper.

4.3.1. Specimens of Series I—End-Bearing Connection

Loading Normal to the Axis of the Supporting Beam

Under tension (pulling) force, the connection bar in end-bearing specimens showed an initial linear elastic stage, followed by a reduction in slope at the onset of bar yielding (Figure 10a). Specimen EB-TN-45 first yielded at 70% of the peak load, which indicates this connection offered ample warning before failure. However, the connection bar in EB-TN-90 experienced less deformation due to the early bond failure of the connection. At the peak load, the measured tensile strains under tension forces with 90-degree (EB-TN-90) and 45-degree bent bars (EB-TN-45) were 2370 and 24,980 με, respectively. The latter tensile strain value confirms that the connection bar in EB-TN-45 reached the necking stage, as mentioned earlier.

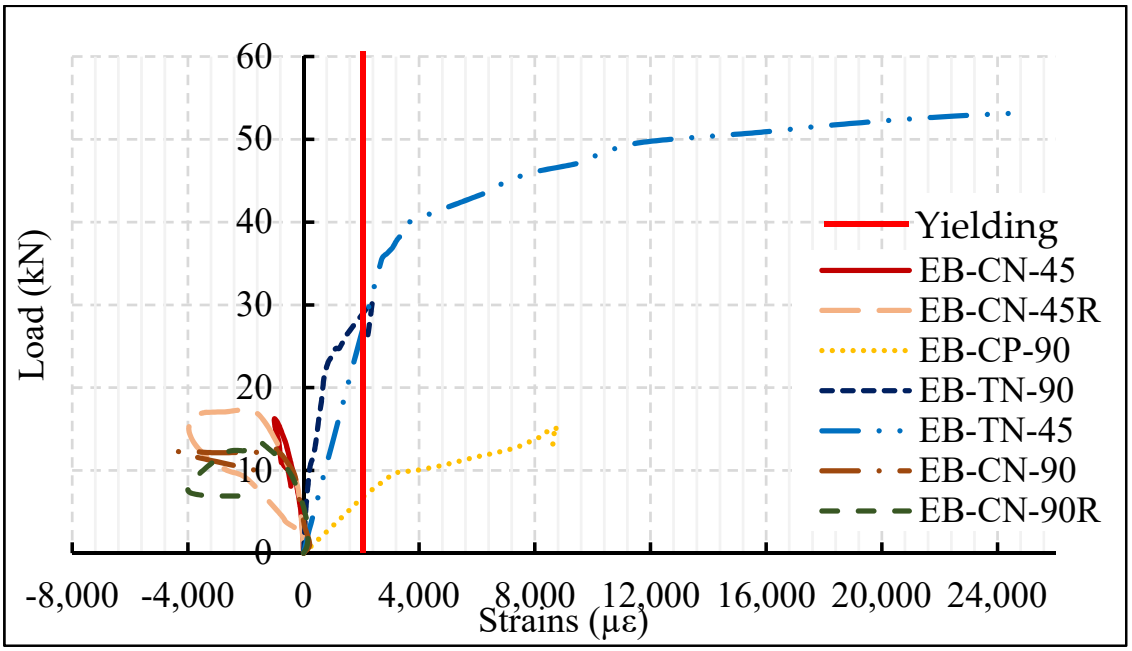

(**a**)

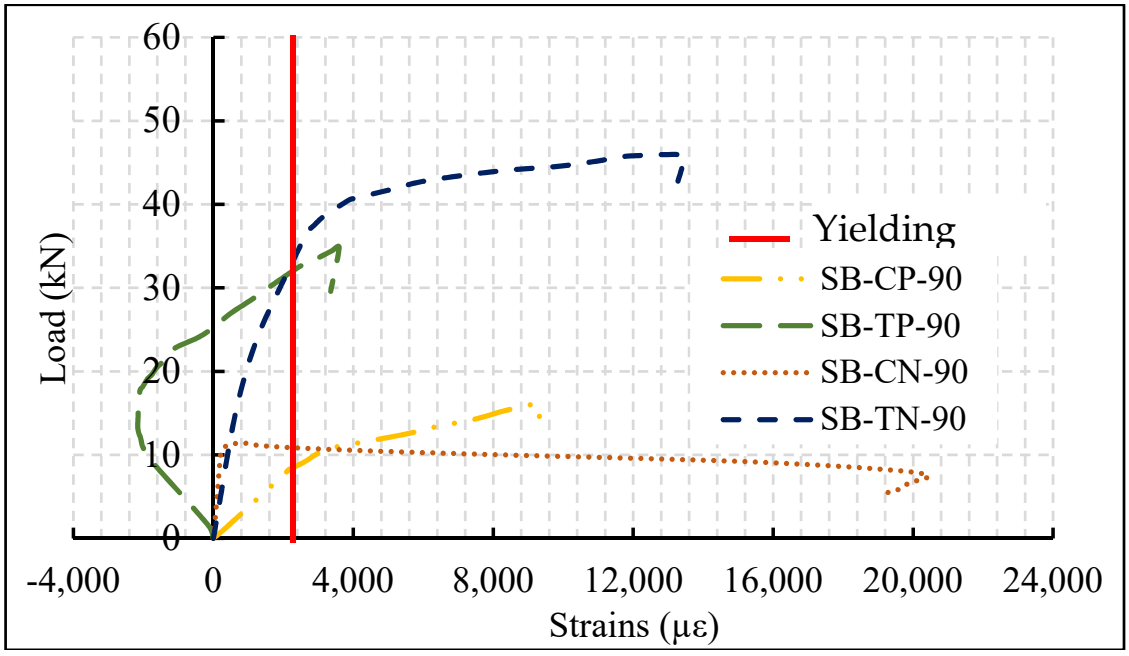

(**b**)

Figure 10. Load-strain relationship for the connection bar at the centerline before the bend: (**a**) Series I—end-bearing specimens, and (**b**) Series II—side-bearing specimens.

Under compression (pushing) forces, the connection bars exhibited an initial linear elastic load-compressive strain behavior, until the onset of bar buckling. Afterwards, the strains significantly increased while the load did not change or gradually dropped, as a result of the bar bending. Finally, the load decreased while the bar suffers further distortion as a result of "dragging" (Figure 10a). For specimens with 45-degree bent bars (EB-CN-45 and EB-CN-45R), the length of the unrestrained bar at the bottom bend in end-bearing connections affected the load-strain behavior. At the peak load, the connection bar in specimen EB-CN-45 attained −1000 με at the bend. After this point of loading, strength degradation was observed along with strain reduction. In contrast, reducing the unrestrained length of the bar in specimen

EB-CN-45R delayed the onset of bar buckling and strength degradation at the bottom bend due to the bar leaning against the top flange of the supporting beam. After the linear elastic stage with compressive strains, the connection bar yielded while buckling near the flange of the supporting beam (Figure 7d). This connection bar maintained the peak load almost steady until approximately −3360 με. Finally, a drop in the load with increasing tensile strains was observed. However, specimens with 90-degree bar bends tested under compression (EB-CN-90 and EB-CN-90R) had no significant difference in their load-strain behavior. At the maximum load, the measured strain in the connection bar in EB-CN-90 and EB-CN-90R, were −1050 and −1460 με, respectively.

Loading Parallel to the Axis of the Supporting Beam

The end-bearing specimen under pushing load (EB-CP-90) showed tensile strains caused by the bar elongation in the direction of the force and bar kinking. The unrestrained bend of the connection bar yielded at approximately 9.1 kN (60% of the capacity). After undergoing significant deformation, bar twisting started at approximately 87% of the peak load and the specimen failed by bar rupture. The maximum strain measured at the unrestrained bend was 8080 με before bar rupture near the welding.

4.3.2. Specimens of Series II—Side-Bearing Connection

Loading Normal to the Axis of the Supporting Beam

The side-bearing specimen (SB-TN-90) under tension force had a similar load-strain relationship to end-bearing specimens. The connection bar of this specimen yielded at approximately 79% of the peak load and reached 13,400 με at the peak load (Figure 10b). On the other hand, when tested under compression forces, the load-strain relationship of the connection bar showed an initial linear-elastic behavior up to bar buckling. According to the strain measured at peak load (900 με), bar buckling does not necessarily mean the bar has yielded. After buckling, strength degradation and tensile strains occurred as an effect of bar drifting by the slab displacement. In the post-buckling stage, the trend of the load-strain relationship for SB-CN-90 and its end-bearing counterparts (EB-CN-90 and EB-CN-90R) agree with the findings of Dhakal and Maekawa [15] and Urmson and Mander [16], where it was reported that the stress–strain relationship depends on the unrestrained length of the steel bar and the bar diameter. As the unrestrained portion of the bar increases, the post-buckling slope is more negatively abrupt. Typically, peak load occurs at yielding or bar buckling [15,16]. Overall, the load-strain relationship of the connection bars tested under compression forces demonstrated that there is no strength gaining after bar buckling.

Loading Parallel to the Axis of the Supporting Beam

The load–strain relationship for the connection bar in the side-bearing specimen (Figure 10b) tested under a pushing force (SB-CP-90) is almost identical to its end-bearing counterpart (Figure 10a). After the initial linear elastic stage, yielding in the connection bar occurred at 60% of the maximum load capacity. At peak load, the measured strain in the connection bar was 9330 με. The side-bearing specimen tested under pulling forces (SB-TP-90) underwent an initial phase of compressive strains since the connection bar was welded at an angle that was not perfectly perpendicular to the flange of the supporting beam. Once the bar straightened, tensile strains occurred until yielding. Finally, the specimen reached a tensile strain of 3350 με at peak load. However, Figure 8d shows neck formation near the welding, which indicates an even larger strain occurred in that portion. Similar to their end-bearing counterpart, bars in side-bearing connections had initially more strain at the same load level, when subjected to parallel (shear) forces compared to specimens that were axially loaded. However, the yielding load under parallel pushing (SB-CP-90, 9.7 kN) and pulling (SB-TP-90, 31.7 kN) was comparable to their side-bearing counterparts (EB-CP-90, 9.2 kN and EB-TP-90, 30.3 kN), respectively.

4.4. Displacements in the Slabs

4.4.1. Specimens of Series I—End-Bearing Connection

Loading Normal to the Axis of the Supporting Beam

End-bearing connections subjected to normal loads had comparable linear elastic load–displacement relationships at the initial stages of loading (where the bar is in the elastic range). The load–displacement graphs diverged at bar buckling for specimens under compression (EB-CN-90, EB-CN-90R, EB-CN-45 and EB-CN-45R); while specimens under tension (EB-TN-90 and EB-TN-45) showed a gradual slope reduction at larger values of load after yielding of the bar.

In specimens under tension, this difference in the slope following the initial elastic stage is associated with the straightening and elongation of the unrestrained bend of the connection bar, and the cracking observed in specimen EB-TN-90. In general, the specimen with a 45-degree bent connection bar (EB-TN-45) exhibited a steeper slope compared to their counterparts with 90-degree bends (EB-TN-90), which implies a stiffer response of the connection. Since the specimen with a 45-degree bend attained 43% more load than the specimen with a 90-degree bend, the connection bar with a 45-degree bend exhibited more stiffness besides the higher load capacity. These two specimens failed at very similar slab displacement (22.6 mm and 21.8 mm in EB-TN-90 and EB-TN-45, respectively). These relatively low values of displacement at failure suggest that the 50 mm seating length is sufficient to avoid loss of bearing of the slabs when the bearing connection bar undergoes tensile stresses.

The load-slab displacement behavior of end-bearing specimens tested under compression forces did not significantly vary with changing the bend angle or reducing the unrestrained length of the bar, as shown in Figure 11a. At peak load, the measured slab displacement of specimens EB-CN-90, EB-CN-90R, EB-CN-45 and EB-CN-45R was 3.9, 4.0, 3.9, and 3.9 mm, respectively.

Loading Parallel to the Axis of the Supporting Beam

The end-bearing specimen (EB-CP-90) tested under pulling force exhibited a linear elastic initial stage, followed by a considerable slope reduction after bar yielding (Figure 11a). A load drop occurred in EB-CP-90 due to bar twisting, which ended with bar rupture. At peak load, the measured slab displacement was 61.5 mm, which exceeded the minimum recommended seating length in the CSA A23.3-19 [5] of 50 mm or ln/180, where ln is the clear span between slab supports. Although there is no potential risk of loss of bearing of the slabs in the side-bearing case, the low stiffness of the connection and the undesirable behavior might result in floor misalignments during construction at relatively low load values.

4.4.2. Specimens of Series II—Side-Bearing Connection

Loading Normal to the Axis of the Supporting Beam

The side-bearing connection tested under axial forces had a similar load-slab displacement relationship (Figure 11b) to their end-bearing counterparts. When subjected to tension forces, specimen SB-TN-90 had a bilinear load–displacement relationship where the connection stiffness reduced at bar yielding. Under compression (pushing) force, the load-slab displacement graph shows an abrupt change after the peak load of specimen SB-CN-90, resulting from bar buckling and loss of capacity (Figure 11b). The curves overlap in the initial linear-elastic stage until the onset of bar bending. Therefore, no significant change in the stiffness can be noted in the pre-peak stage. In addition, the peak load was reached at similar displacements, indicating that there is no significant change in the stiffness of the connection based on the bearing type. On the other hand, the measured displacement of specimen SB-TN-90, tested under tension force, was 22.9 mm at the peak load, while under compression, specimen SB-CN-90 only displaced 3.5 mm when bar bending initiated.

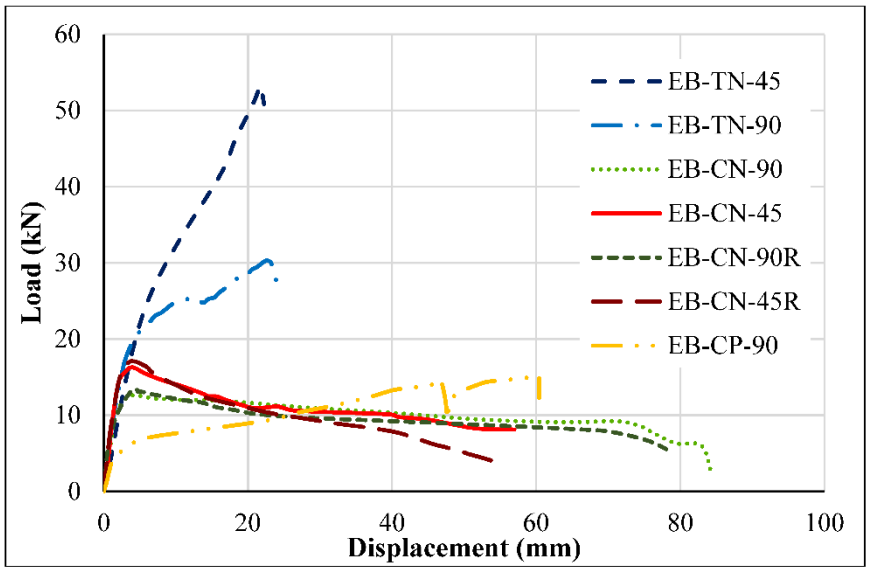

(**a**)

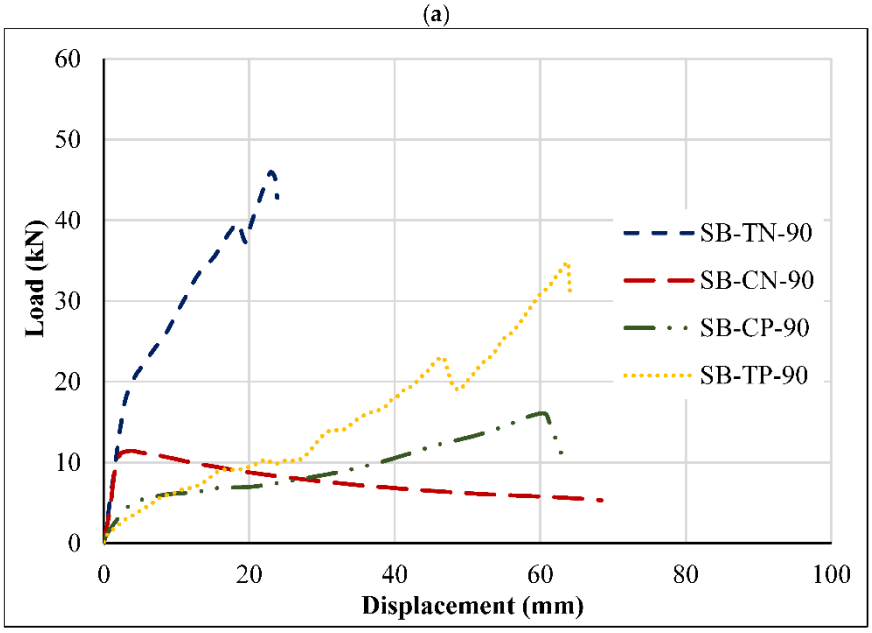

(**b**)

Figure 11. Load-slab displacement relationship: (**a**) End-bearing specimens (Series I) tested under normal and parallel forces, and (**b**) Side-bearing specimens (Series II) tested under normal and parallel forces.

Loading Parallel to the Axis of the Supporting Beam

The side-bearing specimen under parallel pushing force (SB-CP-90) showed a load-slab displacement curve that is similar to the end-bearing specimen EB-CP-90 in terms of the slope at all loading stages (Figure 11b). This indicates no significant variation in the stiffness because of the bearing type.

In contrast, the side-bearing connection (SB-TP-90) under pulling exhibited a steeper load–displacement curve before failure compared to its counterpart tested under a pushing force (Figure 11). Initially, this specimen had a linear-elastic stage followed by a load drop at the onset of the bar twisting. Finally, the load capacity was reached at a displacement of 63.8 mm.

5. Conclusions

Based on the test results of steel connection bars under in-plane forces, the following conclusions can be drawn:

- The connection detailing tested met the minimum tensile capacity specified by the North American standards and codes [4,5] for integrity ties in end-bearing connections under tension forces (normal to the support).
- Specimens tested under tension (pulling normal to support) forces or parallel loads (regardless of load direction) reached yielding or close-to-yielding strains before the peak load. After yielding, the specimens tested under tension forces failed due to grout splitting. However, specimens tested under parallel loads (pushing or pulling) experienced relatively large deformations and yielding under relatively lower loading levels, and no grout or slab cracking was observed after yielding.
- The mode of failure in the specimens tested under compression was governed by bar bending/buckling without yielding, with the exception of specimen EB-CN-45R. Only this specimen was able to reach yielding before peak load, implying an improvement in the mechanism of failure compared to its counterparts with different connection detailing under compression.
- There is no significant difference in the behavior of the end- and side-bearing connections with similar detailing when tested under pushing or pulling forces applied either normal or parallel to the supporting beam.
- The eccentricity in the load path between the applied load and the reaction at the weld triggered the early bending/buckling of the bar at the bend location. Eliminating this eccentricity is expected to increase the connection capacity significantly.

Author Contributions: Conceptualization, E.F.E.-S. and K.M.; methodology, E.F.E.-S., K.M. and S.H.B.; validation, S.H.B., K.M. and E.F.E.-S.; formal analysis, S.H.B.; investigation, S.H.B.; resources, E.F.E.-S.; data curation, S.H.B.; writing—original draft preparation, S.H.B.; writing—review and editing, K.M. and E.F.E.-S.; visualization, S.H.B. and E.F.E.-S.; supervision, E.F.E.-S.; project administration, E.F.E.-S.; funding acquisition, E.F.E.-S. All authors have read and agreed to the published version of the manuscript.

Funding: This research was funded by the Natural Sciences and Engineering Research Council of Canada (NSERC) and the Canadian Precast/Prestressed Concrete Institute (CPCP).

Data Availability Statement: All data, models, and code generated or used during the study appear in the submitted article.

Acknowledgments: The authors wish to express their gratitude and sincere appreciation for the financial support received from the Canadian Precast/Prestressed Concrete Institute (CPCI) and the Natural Sciences and Engineering Research Council of Canada (NSERC). The in-kind contributions received from Armtec Precast (currently, Infrastructure Solutions) and Tower Engineering Group Ltd. are greatly appreciated. In addition, the assistance received from the technical staff of the W.R. McQuade Structures Laboratory at the University of Manitoba is acknowledged.

Conflicts of Interest: The authors declare no conflict of interest.

References

1. Hall, B.J.; Canadian Precast/Prestressed Concrete Institute, Ottawa, ON, Canada. Personal communication, April 2021.
2. Speyer, I.J. Considerations for the Design of Precast Concrete Bearing Wall Buildings to Withstand Abnormal Loads. *J. Prestress. Concr. Inst.* **1976**, *21*, 18–51.
3. CPCI. *CPCI Design Manual*, 5th ed.; Precast and Prestressed Concrete; Canadian Precast/Prestressed Concrete Institute: Ottawa, ON, Canada, 2017.
4. *ACI 318-19*; Building Code Requirements for Structural Concrete and Commentary. ACI 318 Committee; American Concrete Institute: Detroit, MI, USA, 2019.
5. *CSA A23.3-19*; Design of Concrete Structures. Canadian Standards Association (CSA): Toronto, ON, Canada, 2019.
6. PCI. *Manual for the Design of Hollow Core Slabs and Walls*, 3rd ed.; Electronic Version; PCI Hollow Core Slab Producers Committee: Chicago, IL, USA, 2015; Available online: https://www.coreslab.com/wp-content/uploads/2013/07/PCI-Hollowcore-Design-Manual-MNL-116.pdf (accessed on 19 September 2022).
7. Lam, D.; Elliott, K.S.; Nethercot, D.A. Parametric Study on Composite Steel Beams with Precast Concrete Hollow Core Floor Slabs. *J. Constr. Steel Res.* **2000**, *54*, 283–304. [CrossRef]
8. Lam, D. Composite Steel Beams with Precast Hollow Core Slabs: Behaviour and Design. *Prog. Struct. Eng. Mater.* **2002**, *4*, 179–185. [CrossRef]

9. Lam, D. Capacities of Headed Stud Shear Connectors in Composite Steel Beams with Precast Hollowcore Slabs. *J. Constr. Steel Res.* **2007**, *63*, 1160–1174. [CrossRef]
10. Truderung, K.; Tower Engineering Group, Calgary, AB, Canada. Personal communication, January 2019.
11. *ASTM A370-20*; Standard Test Methods and Definitions for Mechanical Testing of Steel Products. American Society for Testing and Materials, International (ASTM): West Conshohocken, PA, USA, 2020.
12. *ASTM C109/C109M-20b*; Standard Test Method for Compressive Strength of Hydraulic Cement Mortars (Using 2-in or [50 Mm] Cube Specimens). American Society for Testing and Materials, International (ASTM): West Conshohocken, PA, USA, 2020.
13. Mejia-McMaster, J.C.; Park, R. Tests on Special Reinforcement for the End Support of Hollow-Core Slabs. *PCI J.* **1994**, *39*, 90–105. [CrossRef]
14. Herlihy, M.D. Precast Concrete Floor Support and Diaphragm Action. Ph.D. Thesis, University of Canterbury, Christchruch, New Zealand, 1999.
15. Dhakal, R.P.; Maekawa, K. Modeling for Postyield Buckling of Reinforcement. *J. Struct. Eng.* **2002**, *128*, 1139–1147. [CrossRef]
16. Urmson, C.R.; Mander, J.B. Local Bucling Analysis of Longitudinal Reinforcing Bars. *J. Struct. Eng.* **2012**, *138*, 62–71. [CrossRef]